AIAA SciTech Forum
6-10 January 2020, Orlando, FL
AIAA Scitech 2020 Forum

10.2514/6.2020-0276

When Higher Fidelity Models Degrade Our Understanding of Induced Drag - The Tragedy of the Trefftz Plane Integral

Timothy T. Takahashi[1]
Che-Wei Ou[2]
Arizona State University, Tempe, AZ 85281

In this work, we show that common wake survey methods cannot differentiate between wings that do or do not develop substantial leading-edge-suction. We point the reader back to the classics and remind him that these derivations fundamentally neglect thickness. That theory is based on the idea that pressure forces always act orthogonal to the airfoil mean-line; thus, they only project normal forces into the drag direction. This means that follow-up theories developed from the Kutta-Joukowski theorem make the same assumption: that wings cannot develop axial forces due to inviscid flow mechanisms. Here, we show how an analytical leading-edge suction correction found in old Vortex-Lattice-Method codes is both accurate and necessary to match test data. Hence, older codes such as VORLAX prove more useful to estimate inviscid drag than do newer wake-integral codes.

I. Introduction

VORTEX Lattice Computional Aerodynamics have been a foundational basis for aircraft design for nearly half a century. In 1971, Margason & Lamar released a NASA Technical Note containing both the method and source code for a computer program that used potential flow techniques to estimate the subsonic aerodynamic characteristics of arbitrary and complex planforms. [1] This program represented the lifting planform with a vortex lattice; [2] which models the aerodynamic shape on an aircraft as a thin sheet which is impermeable to flow. This ultimate expression of thin airfoil theory [3] neglects all thickness effects, yet models the essential aerodynamics of an aircraft with surprising accuracy. Since the Vortex-Lattice-Method is a general method, it enables the aircraft designer to muse as to the effects of variable sweep, to consider changes in dihedral angle across the span, or even a variable dihedral angle near the wing tip, and can model both wings alone as well as wings in the presence of a fuselage body and/or tail. Engineers can effortlessly model even the most complex geometry. These codes run quickly. Vortex-Lattice codes produce all sorts of useful aerodynamic data estimates: lift, drag and side force as well as pitching, rolling and yawing moments. They can estimate surface pressure distributions to support detailed loads estimates. These methods "show good correlation with experimental data." [1] Because Vortex-Lattice-Methods can estimate dynamic derivative (*Cmq, Cnr, Clp*), they transformed the flight dynamics design process and eliminated any need for Etkin style "equation soup" [4].

Vortex-Lattice-Methods are intuitive to use. They are surface panel, as opposed to volume grid, models; thus they need no complex volume mesh generation or refinement to produce quality results.

Vortex-Lattice models have their limitations. They are fundamentally inviscid solution methods; they cannot capture viscous effects. While they may include a Prandtl-Glauert and/or Ackeret [3] model for freestream Mach number effects, none can capture the sharp pressure gradients of shock waves.

Ultimately, Vortex-Lattice-Methods strengths are its greatest weakness. This is because most VLM fundamentally neglect thickness effects. A typical Vortex-Lattice model is a flat-plate "origami"

[1] Professor of Practice, Aerospace and Mechanical Engineering, School for Engineering of Matter, Transport & Energy, P.O. Box 876106, Tempe, AZ, 85281, Associate Fellow AIAA
[2] M.S. Candidate, Aerospace Engineering, School for Engineering of Matter, Transport & Energy, P.O. Box 876106, Tempe, AZ, 85281 Student Member AIAA

representation of an actual aircraft. Some codes allow for a cambered sheet flat panel representation of the lifting surfaces. VORLAX [5] differs from other vortex-lattice models because it has double-impermiable as well as single-impermiable Vortex-Lattice models. In this way, VORLAX can simulated thickness effects if a wing was modelled as a double single-impermiable Vortex-Lattice layer; a "sandwich" panel; see Figure 1. The two layers will interfere with each other and simulate the flow over thick airfoils.

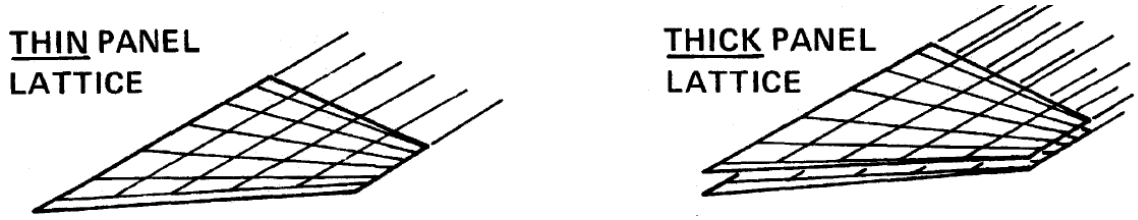

Figure 1 - Thin Double-Impermiable vs Thick Single-Impermiable "Sandwich" Model [5]

While Takahashi is a long time user of Luis Miranda's VORLAX [5], other "newer" Vortex-Lattice codes have become popular with other designers; among them AVL [6] VLAERO [7] and Tornado [8]. Some of these "newer" codes use a different approach to drag calculation than Margarson [1] or Miranda [5]; and with no surprise to many readers, it is the newer codes not VORLAX that gives Takahashi heartburn.

Here is an example of the problem.

In AIAA 2016-0776, [9] El Haddad and Gonzalez designed a winglet for a Dassault Falcon 10 business jet. They use Vortex-Lattice-Methods is a fairly typical manner. First, they conceptualized twelve combinations of winglet cant angle and winglet semi-span. They develop a multi-disciplinary model to identify which one provided the best compromise between induced drag reduction, zero-lift-drag penalty and structural weight increase. VLAERO was the core aerodynamics model they used to explore the design space. They followed up this with a detailed design loads analysis performed using a Reynolds–Averaged Navier–Stokes (RANS) CFD model. All of these seems eminently reasonable.

My heartburn begins as I learn more about the level of accuracy found with this commercial code. VLAERO [7] incorporates the Prandtl-Glauert compressibility correction; no problem there. But VLAERO uses a Trefftz-plane wake-integration model to calculate induced drag. And here the users needed to apply " a calibration factor ("Trefftz factor") of 1.2" to match wind tunnel data. [9] So to be clear, there is a 20% error in drag-due-to-lift arising in their fundamental analysis code, yet they use this same code to support decision making where they downselected a specific winglet geometry that provided only a 2.5% reduction in overall drag.

Where is the source of their problem? Is the problem a result of poor conceptual approach to the winglet design (their method seems reasonable to me) or is it due to problems with the Trefftz-plane wake-integration model (this problem seems obvious to me)?

In this paper, we show why the supposedly "obsolete" analytical leading-edge-suction method of Margarson [1] and Miranda [5] is functionally superior to the more sophisticated Trefftz-plane method. The source of the disconnect is that there is a marked influence of the leading-edge shape of the wing on drag; and that these effects are only seen in near-field (as opposed to the Trefftz-plane far-field) flow field. We suggest that the wake survey (whether physical or virtual) is an inappropriate means to infer lift-induced drag.

We examine the problem by looking at Computational Fluid Dynamics (CFD), Vortex-Lattice potential flow code (VORLAX), and wind tunnels data for a variety of wings. To no surprise, we find that sharp leading-edge wings have less leading-edge suction and higher drag than blunt leading-edge wings; but to our consternation, we find that the very real impact leading edge geometry has on drag does not express itself clearly in the wake.

We concur with the belief that Vortex-Lattice-Methods should remain a cornerstone of aerodynamic analysis for aircraft conceptual and preliminary design. We show how, in particular, VORLAX [5] truly captures the essential flow field developed by low aspect ratio wings. At the same time, we demonstrate good reason for our concern over the drag model found in certain other popular codes.

II. Observations on Induced Drag

"Induced drag is an evil, because all drag is an evil, but it is a necessary evil at least and expended for something we want," said Max Munk [10]. There are many sources of drag, but induced drag is the most inevitable byproduct of lift generation. In classical aerodynamics, induced drag increases with the square of the lift. The classical theory developed by Munk [10] considered the induced drag as a direct byproduct of the production of downwash whereas Mclean [11] defines induced drag strictly in terms of the energy loss imparted into the disturbed wake flow. We will see throughout this paper how these two approaches produce differing estimates of drag.

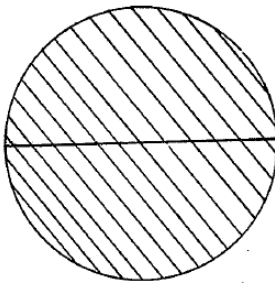

Figure 2: Max Munk's Circular Downwash Influence Model [10]

A. Induced Drag is the Drag Due to Lift; Don't Forget that Downwash Produces Lift

Munk [10] proposed that a lifting wing generates lift because it deflects the oncoming air flow downwards. Thus, lift can be calculated as the change in momentum due to the downwash velocity. In his statement, the downwash area affected by wings must be the same as the span of the wings. The air flowing through the shaded area is shown in Figure 2.

$$L = \dot{m} V_d \tag{1}$$

Where V_d is the downwash velocity and $\dot{m}$ is the mass flow rate through the circular area shown below as:

$$\dot{m} = \frac{1}{4}\pi b^2 V_\infty \rho \tag{2}$$

Where b is the wing span, V_∞ is the freestream velocity, and ρ is the air density.

Why is the area of influence the cross sectional area of the shaded cylinder? (1/4 span squared times π?) According to Munk, it was his colleague Pohlhausen's idea [12] [13] , but our extensive literature search hasn't found a rigorous derivation.

Munk continues to determine that the kinetic energy through this region can simply be defined as:

$$KE_d = \frac{1}{2}\dot{m} V_d^2 = \frac{1}{2} * \frac{L^2}{\dot{m}} = \frac{L^2}{\frac{1}{2}\pi b^2 V_\infty \rho} \tag{3}$$

Following the work-energy theorem, drag can be defined in terms of the kinetic energy changes in the "wake" flow behind the wing.

$$D_i = \frac{KE_d}{V_\infty} = \frac{L^2}{\pi b^2 q_\infty} \tag{4}$$

where $q_\infty = \frac{1}{2}\rho V_\infty^2$ is the incompressible freestream dynamic pressure.

To convert these forces into coefficient form, we use the following relationship, $AR = b^2 / Sref$, (where AR is the aspect ratio of the wing and substituting this into equation 4. We then dividing both sides by $q\ Sref$ to obtain the induced drag in coefficient form:

$$C_{D_i} = \frac{D_i}{q * S_{ref}} = \frac{L^2}{\pi * AR * (q * s_{ref})^2} = \frac{C_L^2}{\pi * AR} \tag{5}$$

Note that Munk's basic method does not accurately calculate the induced drag for non-elliptical loadings. In addition, his method does not consider the effect of the nuanced thickness or camber of the wing. Indeed, we speculate that Munk's method (the Pohlhausen cylinder of downwash) was contrived to fit experimental data for blunt leading-edge wings with elliptical transverse span loads.

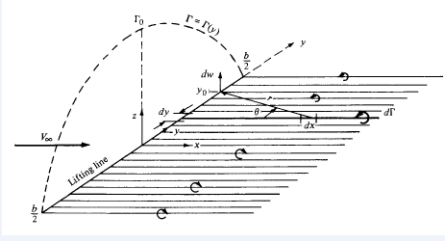

Figure 3 - Prandtl Lifting Line Theory

B. The Joukowski Transformation Introduces Error into Our Understanding of Induced Drag

Anderson [14], as well as Bertin & Cummings [15], also derive induced drag from the downwash velocity field, but in the context of Prandtl's lifting line theory. [16] Prandtl, in turn, determines lift from the circulation of the spanwise vortices shown in Figure 3.

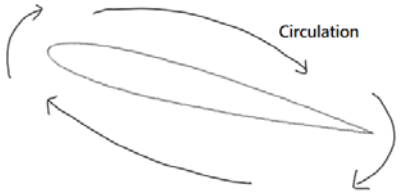

Figure 4 -Circulation around an airfoil section

Given there is a limitation with the circulation defined along the span, with the range of $-\frac{b}{2}$ to $+\frac{b}{2}$, each spanwise component of lift is defined via the Kutta-Joukowski theorem:

$$L'(y_0) = \rho_\infty V_\infty \Gamma(y_0) \tag{6}$$

Where Γ is the circulation (see Figure 4) and y_0 is a specific transverse "strip" on the span.

Observe that Kutta-Joukowski theorem is composed of two parts: the Kutta condition and the Joukowski transformation. The Joukowski transformation [17] states that the flow around a cylinder can be transformed into flow around airfoil-like shape with a round leading-edge and a sharp trailing edge. From the Kutta condition the theorem can be applied to analyze a "sharp" trailing edge airfoil. Therefore, the Kutta-Joukowski theorem does not consider the thickness or camber effect because the force acting on the surface are assumed to point to the center of the airfoil instead of normal to the surface. (see Figure 5, overleaf) Also, the theorem can only be applied to blunt leading-edge airfoils because of the Joukowski transformation.

Going back to the derivation of Lifting Line Theory, classical theory [3][14][15][16][18][19] states that the total lift is simply an integration of the spanwise lift function:

$$L = \int_{-\frac{b}{2}}^{\frac{b}{2}} L'(y)dy = \rho_\infty V_\infty \int_{-\frac{b}{2}}^{\frac{b}{2}} \Gamma(y)dy \tag{7}$$

Or, in coefficient form:

$$C_L = \frac{2}{V_\infty S_{ref}} \int_{-\frac{b}{2}}^{\frac{b}{2}} \Gamma(y)dy \tag{8}$$

Due the downwash velocity V_d not being parallel with the freestream velocity V_∞, there is an induced angle of attack, α_i , that alters the effective angle-of-attack, α_{eff}, of the airfoil section.

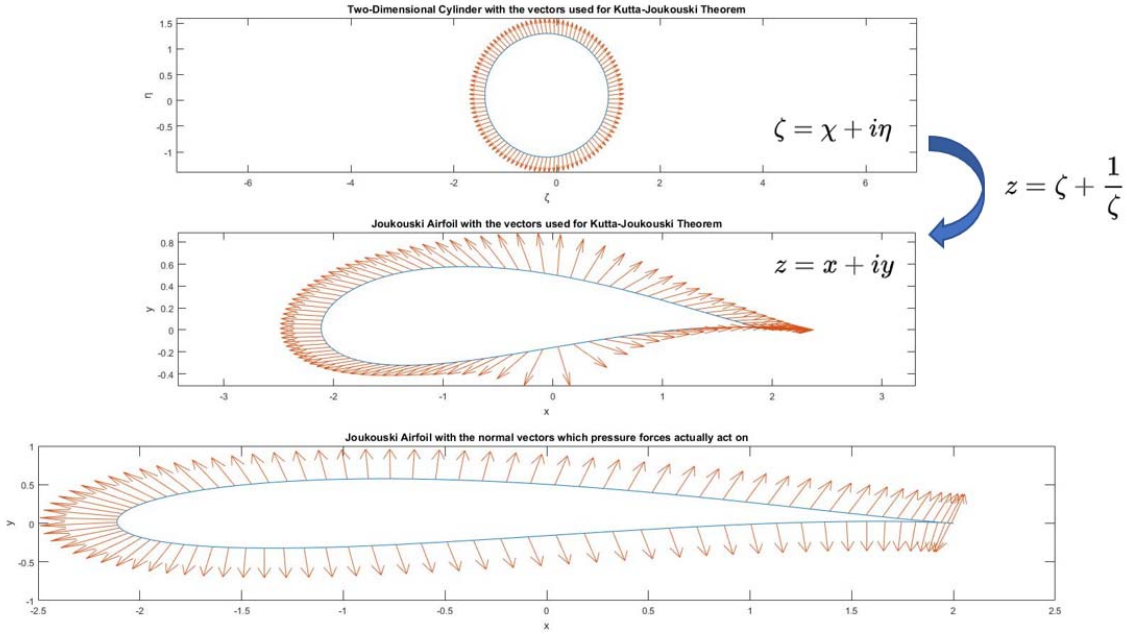

Figure 5 - The Difference between the Joukowski Transformation and pressures acting upon a Real Airfoil

For small angles where $tan\,\alpha \approx \alpha$ (in radians), the induced angle of attack can be defined as follows:

$$\alpha_i(y_0) = \frac{-V_d(y_0)}{V_\infty} \tag{9}$$

Note that the concept near-field lift is a approach to simplify two-dimensional airfoil theory to "work" in the context of a finite wing. Moreover, the induced drag D_i derived in Figure 6 represents the local transformation of axis of only the normal force of the 2D airfoil. This approach neglects any viscous or inviscid contribution from axial forces in the underlying 2D model!

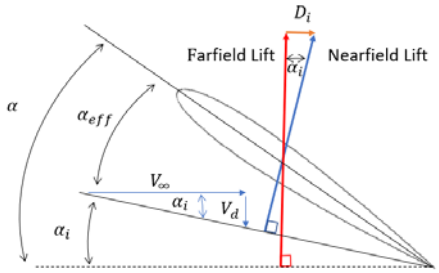

Figure 6 - Downwash Angle and Induced Angle of Attack

In this derivation, downwash velocity is defined as the effect of all vortices on a single point on the span:

$$V_d(y_0) = -\frac{1}{4\pi}\int_{-\frac{b}{2}}^{\frac{b}{2}} \frac{1}{y_0 - y}\frac{d\Gamma}{dy}dy \tag{10}$$

which is substituted into Equation (9) to calculate induced angle of attack purely based on freestream velocity and circulation:

$$\alpha_i(y_0) = \frac{1}{4\pi V_\infty}\int_{-\frac{b}{2}}^{\frac{b}{2}} \frac{1}{y_0 - y}\frac{d\Gamma}{dy}dy \tag{11}$$

The drag due to lift at each spanwise point can then be calculated as the streamwise component of the normal force vector at this induced angle of attack, which again is assumed to be negligible so $sin\,\alpha_i = \alpha_i$:

$$D_i'(y_0) = L'\,sin\,\alpha_i(y_0) = L'\alpha_i \tag{12}$$

Substituting the spanwise lift from Equation (12) and following the same mathematical logic of integration across the span results in the following equation:

$$D_i = \rho_\infty V_\infty \int_{-\frac{b}{2}}^{\frac{b}{2}} \Gamma(y)\alpha_i(y)dy \tag{13}$$

Which in coefficient form becomes:

$$C_{D_i} = \frac{2}{V_\infty S_{ref}} \int_{-\frac{b}{2}}^{\frac{b}{2}} \Gamma(y)\alpha_i(y)dy \tag{14}$$

If we assume that the transverse lift distribution is "elliptical" and a function of the reference circulation Γ_0, we can derive:

$$C_{D_i} = \frac{\pi\alpha_i\Gamma_0 b}{2V_\infty S_{ref}} = \frac{\pi b}{2V_\infty S_{ref}}\left(\frac{C_L}{\pi AR}\right)\left(\frac{2V_\infty S_{ref} C_L}{b\pi}\right) \tag{15}$$

Which reduces to:

$$C_{D_i} = \frac{C_L^2}{\pi AR} \tag{16}$$

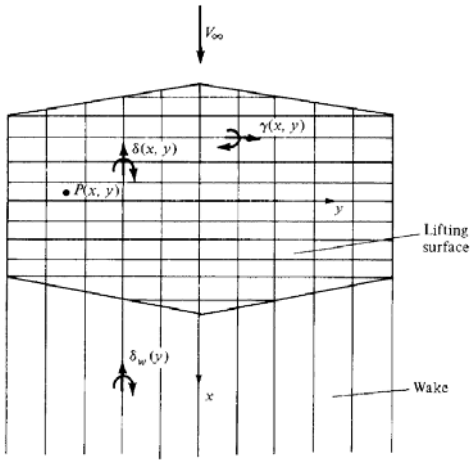

Figure 7 – Multhopp's Lifting Surface Theory

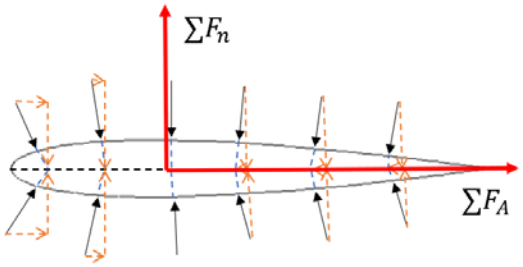

Figure 8 – Discrepancies between thin-sheet and real airfoil pressure

Finally, let us move on the Multhopp's Lifting Surface Theory [20]; see Figure 7. Multhopp's method anticipates the Vortex-Lattice-Method. [5] His approach differs from the Lifting Line Theory because he treats circulation and downwash as a function of spanwise location **and** chordwise location. This will prove an essential novation as we consider the implications of how thickness impacts the pressure drag of the wing.

Thus, we see that all of these methods to find "induced drag" do not account for any geometry-dependent leading-edge suction despite the whole leading-edge-suction phenomenon being well known in other classic texts (e.g. Bertin & Cummings [15] or Katz & Plotkin [16]).

Classical theory considers a world where the induced drag is solely a function of the circulation distribution. It neglects any contributions to drag arising from the nuanced thickness or camber profile of the wing. It isn't even internally consistent: in Figure 8, we can see the distinctions between a real wing (where pressure forces act normal to the local surface) and the assumption that all pressure forces act normal to the wing reference plane. Moreover, since the Joukowski transformation does not represent either paradigm, the theoretical foundations of the "ellpitical" lift distribution are not as rigorous as we would hope for.

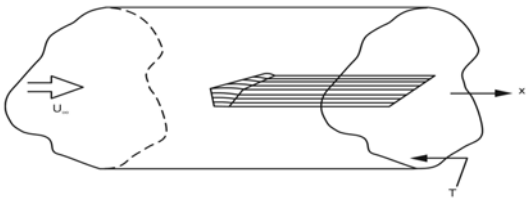

Figure 9 - The Concept of Trefftz Plane after Mclean [11]

C. The Lift Dependent Drag Expressed into the Far-Field Wake May Not Be the Real Induced Drag Either

We can also consider the drag of the wing as being related to the energy imparted into the downstream flow, at a "cutting plane" S_1 which is called the Trefftz plane; see Figure 9. McLean [11] noted that the

bound vorticity found in the wing trails downstream as "filaments." Following the Kutta-Joukowski theorem, there must be some force developed orthogonal to these far-field velocity and vorticity vectors; they are the lift and induced drag.

Mclean's proposes a direct method based on this control volume analysis:

$$D_i = \iint_{S_1} \frac{1}{2}\rho\left(-u_{1_i}^2 + v_{1_i}^2 + w_{1_i}^2\right)dS_1 \tag{17}$$

Which captures the difference in kinetic energy between the upstream and downstream wake flow. Superficially, it appears to be a direct method that would infer energy losses in the control volume.

Another, more popular, method comes from 1972. [21]20][23][24] Maskell [21] described a method to decompose the induced drag and viscous drag and presented them by velocity potential function and stream function in three-dimensional space.

Takahashi [26] noted that Maskell [21] defines Betz's two-dimensional formula [25] as the profile drag and combines it with a three-dimensional kinetic energy loss term:

$$D = \int\int [(P_\infty - P) + \frac{\rho}{2}(u^* - u)\left(u^* + u - 2(U_\infty + u_b)\right)dS + \frac{\rho}{2}\int\int (v^2 + w^2)dS \tag{18}$$

The first integral term presents the viscous drag and the second integral term is the cross-plane vortex-drag term:

$$D_i = \frac{\rho}{2}\int\int (v^2 + w^2)dS \tag{19}$$

Maskell [21] innovates and suggests that we replace v and w with the stream function and velocity potential function

$$v = \frac{\partial \Psi}{\partial z} + \frac{\partial \phi}{\partial y}, w = -\frac{\partial \Psi}{\partial y} + \frac{\partial \phi}{\partial z} \tag{20}$$

After considerable mathematical manipulation, Maskell [21] derives :

$$D_i = \frac{\rho}{2}\int\int \Psi\xi dS - \frac{\rho}{2}\int\int \phi\sigma dS \tag{21}$$

However, to infer stream function Ψ and velocity potential function ϕ from test data (u,v,w wake flow velocity measurements), we must solve the Poisson's equation [21] using a numerical method.

Maskell's method [21] is peculiar because it basically requires the analyst to infer the potential flow terms from the real flow only to re-use these terms in the contrived classical derivation. While Brune and assoicates [22][23], claim great accuracy with this method; it seems restricted for applications where the classical lifting line theory identically matches experiment.

D. Pressure Loops Demonstrate the Interaction Between Circulation and Leading-Edge-Suction

Following basic geometry, we can see that lift and drag are functions of both the normal and axial forces developed by the flow as it interacts with a wing.

$$L = N\cos(\alpha) - A\sin(\alpha)$$
$$D = N\sin(\alpha) + A\cos(\alpha) \quad (22)$$

Leading-edge-suction is an axial (or drag direction) force contribution due to the interaction of the nuanced thickness, incidence and camber profile of the wing, and the local surface pressures resulting from flow over this surface.

Here, we will demonstrate that on blunt leading-edge wings the axial pressure force due to lift opposes the axial tractions due to skin friction.

Recall that pressure forces act perpendicular to the wetted surface. In other words, pressure works on each mesh element in a direction normal to wetted surface. In Figure 10, we show the normal vectors along the surfaces of a NACA 0012 airfoil. The reader can see that the arrows lean heavily into the axial direction near the leading-edge.

Thus, armed with basic airfoil geometry, we can thus compare and contrast the impacts of equally thick blunt and sharp leading edge thickness forms.

Turn to Figure 11, and compare the NACA 4-digit form to a biconvex form. In Figure 12, we compute the direction cosines and sines from the geometry at zero angle of attack – these values represent the fraction of the pressure acting in the direction normal or axial to the airfoil reference chord. While the integration of this value produces a value close to 1, it is not exactly 1. Thus, airfoils can produce a "pressure drag" or "pressure thrust" even in the absence of sonic or separated flow.

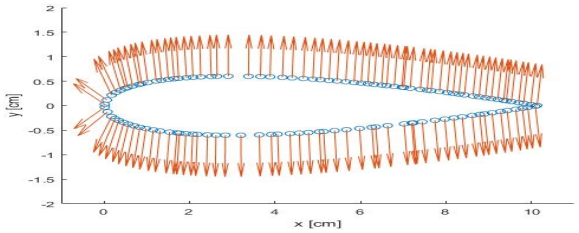

Figure 10 - Normal Vector for the Middle Point of Each Panel.

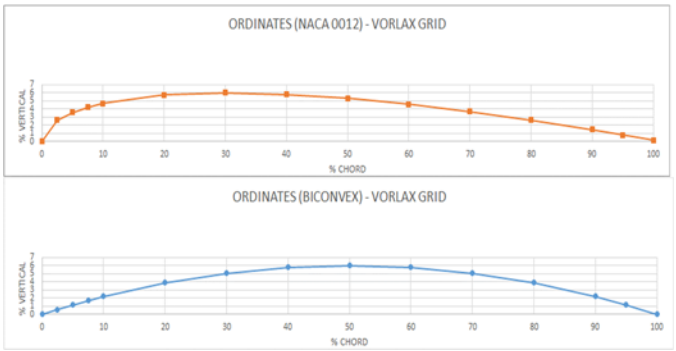

Figure 11 - NACA 0012 and Biconvex Airfoil Coordinates

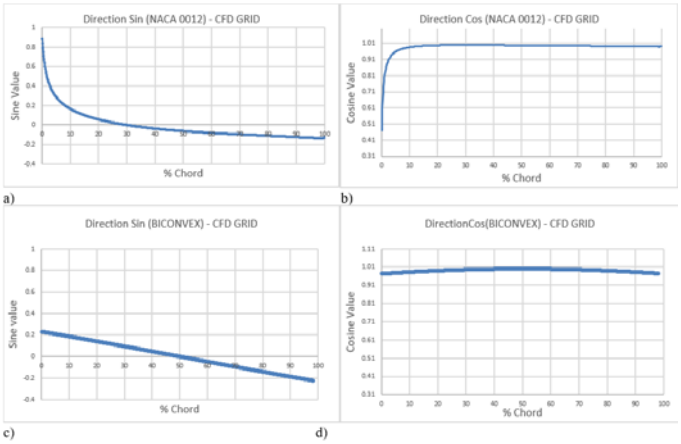

Figure 12 - Comparison of Cosine and Sine Components for the Normal Vector of the Mesh Panels Between a NACA 0012 Airfoil and a Biconvex Airfoil.

The blunt leading-edge case in Figure 12a and 12b indicates that the pressure forces near the leading edge contribute to axial force, which we know that is source of leading-edge-suction (our "negative pressure drag"). On the contrary, the sharp leading-edge in Figure 12c and 12d demonstrates a reduction in axial force contribution from the pressure field that is solely due to the leading-edge geometry.

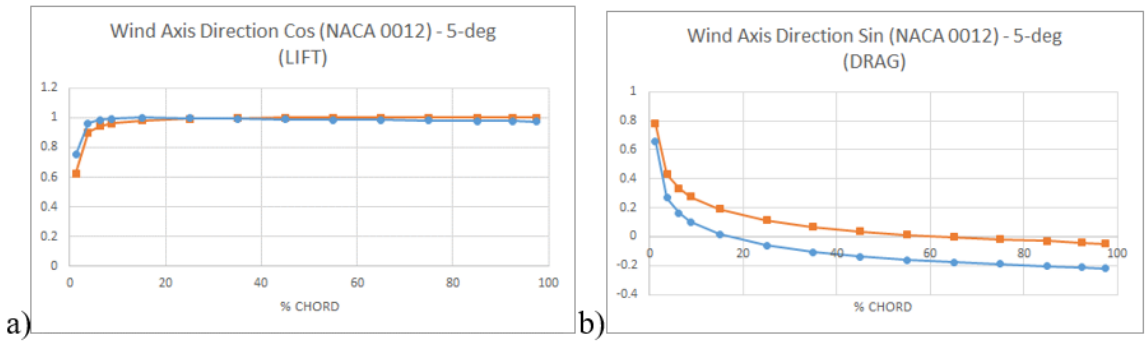

Figure 13 - Direction Cosines NACA 0012 Airfoil at 0 vs 5-degrees Angle of Attack

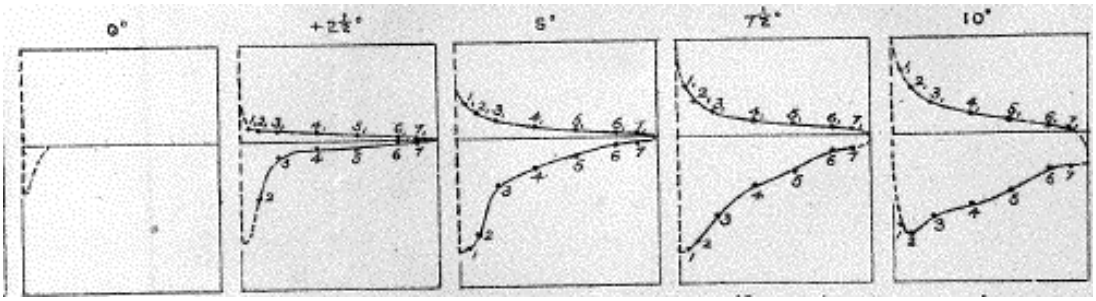

Figure 14 - Classical CP vs Chord Plot (from ARC R&M 60)

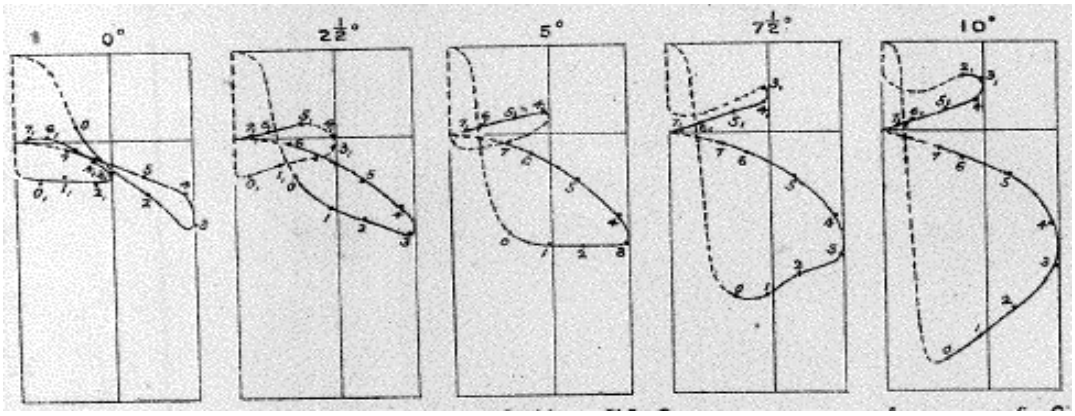

Figure 15 - Suction Loop CP vs Z' Plot (from ARC R&M 60)

In Figure 13, we recompute these direction sines and cosines for the 0012 airfoil, now at 5° angle of attack. Here the inclined airfoils exhibit even stronger axial contribitions (both with (for negative direction cosines) and against the (for positive direction sines) oncoming flow). In this way, airfoils produce an angle-of-attack dependent "pressure drag" or "pressure thrust" even in the absence of sonic or separated flow.

This effect was originally noted by the Bairstow & Jones in ARC R&M 60 from 1914 [27], over 100 years ago. Unfortuately, these effects were not directly incorporated into either Prandtl's or Multhopp's famous theories.

Bairstow & Jones' novation was that instead of producing a *Cp* vs chordwise location pressure plot (see Figure 14), we consider the projection of the pressures in terms of the wind-axis frontal area of the lifting surface (see Figure 15). From a visual inspection, the reader can see that the net contribution of the thickness form to axial force is signficiant.

III. Experiment and Computation Substantiate This Heresy

In this section we will compare vortex-lattice results against CFD and wind-tunnel data. Mr. Ou modelled a finite aspect ratio (AR=3) NACA 4-digit and biconvex wing in both VORLAX (flat panel), VORLAX (sandwich panel) and in AutoDesk CFD 2018 using a *SST k-omega RC* (Smirnov-Menter) turbulence model. We compared these results against undergraduate student collected wind tunnel data made for a similar NACA 4-digit wing. [29][30] VORLAX [5] is, by nature, inviscid. We ran our CFD to match wind-tunnel Reynolds and Mach number conditions (Re# = ~150,000, Mach# = ~0.07) [29][30] and used the default adaptive grid solver. Our VORLAX model had a grid density of 100 spanwise and 20 chordwise elements.

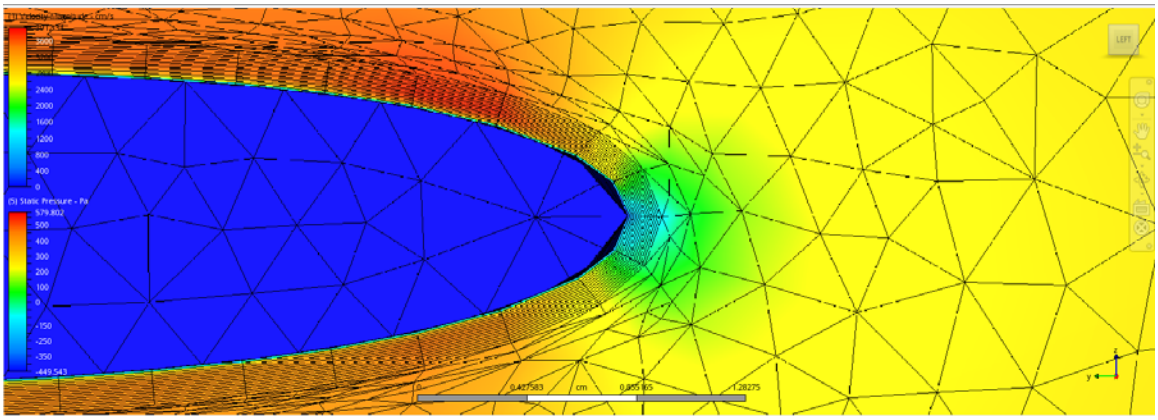

Figure 16 - CFD grid – showing boundary layer

A. Analytical Corrections as used in VORLAX Properly Capture Blunt and Sharp-Leading-Edge Suction Forces

VORLAX computes lift, drag and moments by a combination of direct surface pressure integration and an analytical leading-edge suction "correction."

The VORLAX analytical leading-edge-suction correction follows Lan's procedure [31]:

$$C_t = \pi C^2 \frac{\left(1-M_\infty^2 \cos^2 \Lambda\right)^{\frac{1}{2}}}{2 \cos \Lambda} \tag{23}$$

where C is a function of the strength of the bound-vorticity at the leading edge, Λ is the sweep angle and the leading-edge-suction force correction follows the Prandtl-Glauert rule as applied to the Mach number normal to the leading edge. VORLAX treats the leading edge suction as the axial force when computing lift and drag. A blunt leading-edge can be simulated by setting the "SPC" parameter equal to 1 (applying 100% of the analytical correction); wherease a sharp leading-edge can be simulated using a lower value of this parameter (reducing to zero correction).

In Figure 17 (overleaf), we can compare the relative accuracy of our methods as applied to an AR=3 NACA 4-digit airfoil wing as tested at the ASU wind tunnel. In Figure 17a we see that the wind tunnel, the viscous CFD model and the VORLAX models (flat panel and sandwich) all match extremely closely when predicting lift. The effect of the analytical leading-edge-suction term on lift is negligable. However, when we turn to Figure 17b and examine the axial force prediction, we can see that both our viscous CFD model and the VORLAX model with 100% analytical leading-edge-suction correction closely match experiment. Thus, we can see that the analytical leading-edge-suction model accurately captures the real world effect of blunt airfoils. Putting things together and looking at the drag polars of Figure 17c, we see that the 100% analytical-leading-edge-suction corrected VORLAX run produces a "CFD quality" drag-due-to-lift polar. As we reduce the amount of leading-edge-suction, drag-due-to-lift markedly increases.

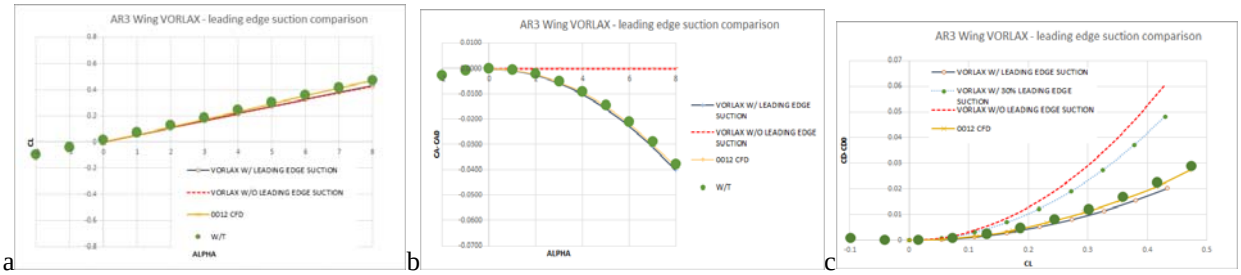

a b c

Figure 17 – Comparison of Experiment and Computation for NACA 4-digit sections – a) Lift vs α; b) Axial Force vs α, c) Drag vs Lift

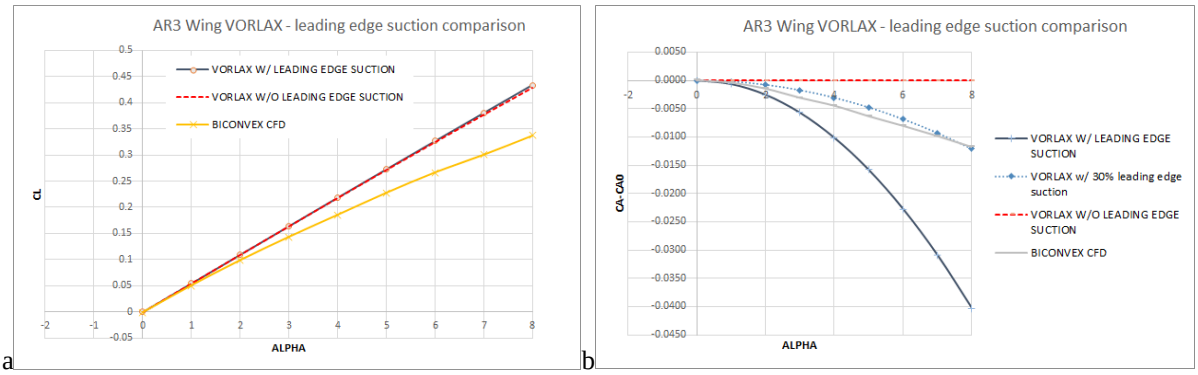

a b

Figure 18 – Comparison for Biconvex sections – a) Lift; b) Axial Force

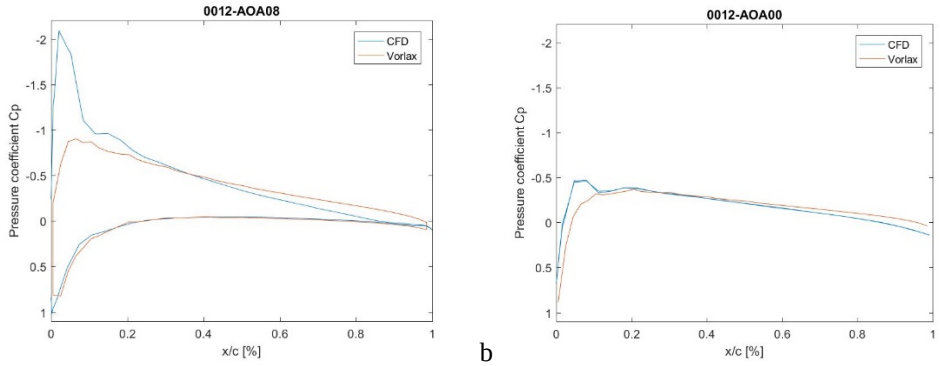

a b

Figure 19 – Mid-Span Pressure Profile – NACA 4-digit Airfoil

In Figure 18, we can compare the relative accuracy of our methods as applied to an AR=3 Biconvex section. In Figure 18a we see that the viscous CFD model and the VORLAX model don't match as well – premature flow separation in the viscous model depresses the slope of *CL* vs α. In Figure 18b we can see that viscous CFD model can be best approximated by the VORLAX model with only 30% analytical leading-edge-suction correction. Thus, we can see that the analytical leading-edge-suction model can be "tuned" to approximate the real world effect of sharp-edge airfoils.

B. VORLAX correctly captures the Chordwise Pressure Distribution

Here, we examine how well a VORLAX "sandwich" panel captures the chordwise pressure field created by the wing. In Figures 19 and 20, we see the chord-wise pressure distribution along the center-line of our AR=3 wing for both the blunt leading-edge NACA 0012 and the sharp leading-edge model, biconvex wing.

Turn first to Figure 19, here we see that the coarse grid VORLAX sandwich panel model accurately resolves the pressures due to thickness of the 0012 form at zero-lift; and largely captures the pressure profile at

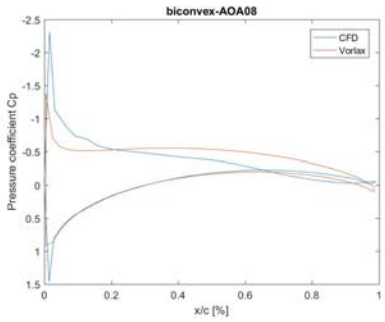

Figure 20 – Mid-Span Pressure Profile – Biconvex Airfoil

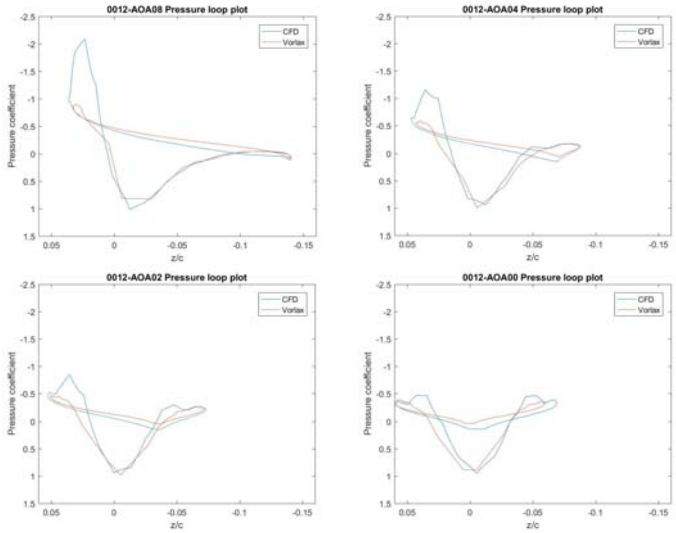

Figure 21 - Pressure Loops for NACA 0012 Airfoil

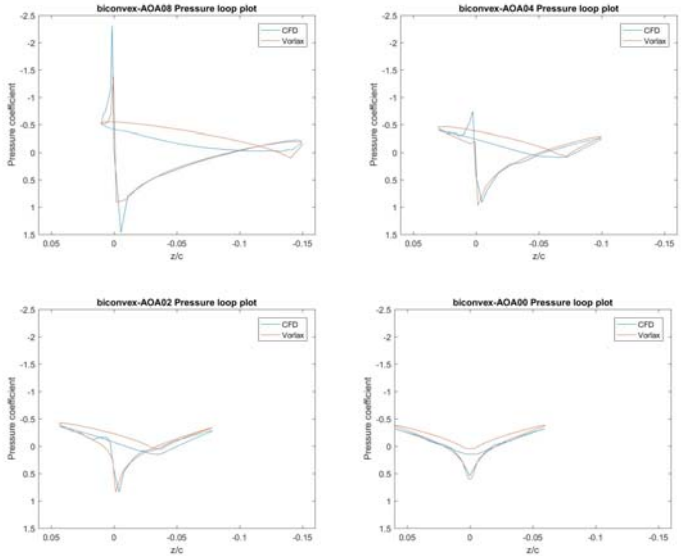

Figure 22 - Pressure Loops for Biconvex Airfoil

α=8°. The source of discrepancy between the methods is found near the leading-edge, with the coarse-grid VORLAX model under-predicting the magnitude of the suction spike.

For the biconvex airfoil in Figure 20, we see that the CFD model shows a very strong suction spike at the sharp leading edge followed by a rapid deceleration which may result in some flow separation. The VORLAX model, with its coarse grid, doesn't resolve the leading-edge suction "spike" as clearly as the CFD model; pressures differ elsewhere on the airfoil. Hence the quality of lift prediction from VORLAX for these separation prone airfoils is worse than for more benign, blunt leading-edge sections.

C. Pressure Loop Plots Verify the Presence of Leading-Edge Suction in Both CFD and VORLAX Solutions

Turn next to Figures 21 and 22, where we compare pressure loop plots developed from the surface pressure computations made using viscous CFD and VORLAX sandwich panel models at α = 0°, 2°, 4° and 8°. Here we see the essentially broad features of the two models – the distinction between airfoil shape and grid density.

The blunt leading-edge airfoil in Figure 21 exhibits a classical "pressure loop" similar to that noted by Bairstow & Jones [27]. If the pressure value is negative, it produces suction forces to pull the airfoil forward. On the contrary, the positive pressure is drag force res isting the forward force. Moreover, the area surrounded by the curve indicates the total suction force if the area is in negative region or drag force if the area is in positive region.

On the contrary, the sharp leading-edge cases of Figure 22 produce a

markedly different form. Comparing these to the 4-digit airfoil, we see that biconvex airfoil has almost no suction force. Even looking at the highest angle of attack case (α=8°), the area of suction force remains smaller than the blunt leading-edge airfoil. It shows that the same airfoil with identical chord length, thickness, and camber will develop markedly different axial forces due to nuance in their respective leading-edge geometry. Within each figure, we can see that features of the "suction loops" near the leading edges are poorly captured by the coarse grid of the VORLAX sandwich panel model. In the case of the NACA 4-digit airfoil, these differences will manifest themselves as a large error in axial force integration associated with the VORLAX model. In the case of the biconvex form, the errors are much smaller. Thus, these two wings exhibit wildly different drag-due-to-lift characteritics because leading-edge geometry has such a strong effect upon leading-edge suction.

Hence, we show that the VORLAX analytical leading-edge-suction model works well for thin, flat-plate models and demonstrate why a coarse-grid VORLAX sandwich panel model is unusable to directly compute leading-edge-suction and hence drag-due-to-lift.

D. VORLAX captures the transverse span loads for fully attached flows

Lifting line theory correctly identifies the impact of transverse span loads upon the induced drag of a wing. While the smooth, "elliptical" distribution sheds bound vorticity gracefully, a lumpy span load that develops the same aggregate lift will shed counter-rotating vorticity into the wake and hence have higher vortex-drag than the ideal.

In Figure 23, we show how well VORLAX sandwich panel models capture the transverse lift distribution of the NACA 0012 wing. The CFD and VORLAX sandwich panel models are essentially similar, except at the extreme wingtip – where there is some flow separation evident in the CFD.

In Figure 24, we show that the VORLAX sandwich panel models perform increasingly poorly at higher angles of attack when modelling the Biconvex section. Here the CFD models predict significantly less lift than does VORLAX. Although the qualitative shape of the pressure distributions seen in Figure 20 do not look that different, lift represents the integration of the difference between upper and lower surface pressures. As the angle-of-attack increases, leading-edge flow separation worsens, and the quantitative solutions diverge from one another.

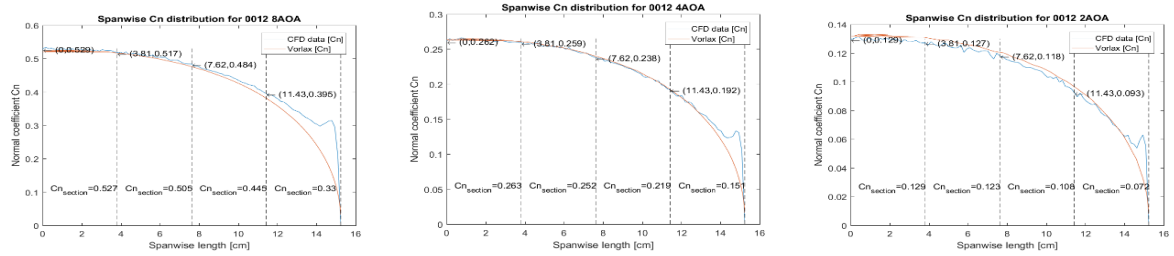

Figure 23 – Transverse Span Loads for NACA 0012 Airfoil

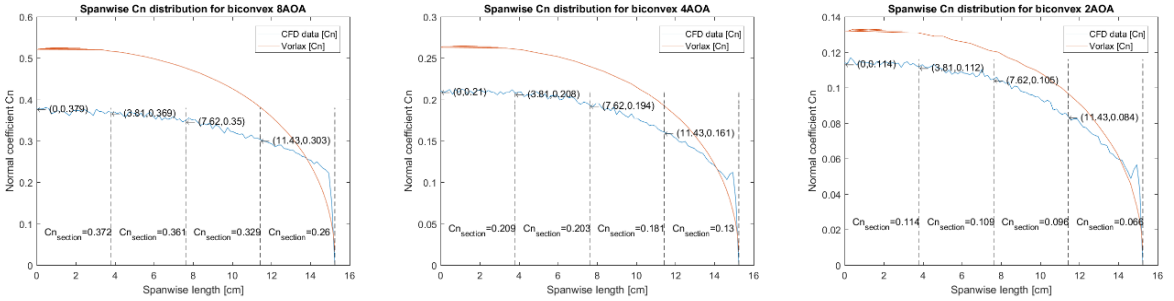

Figure 24 – Transverse Span Loads for Biconvex Airfoil

E. VORLAX is very useful, but sandwich panels are unsuitable to estimate induced drag

Putting all of these observations together, we see that:

1. The nuanced shape of the leading-edge affects flow separation, when flow remains attached the VORLAX model (flat sheet or "sandwich panel") accurately predicts the lift, transverse span load and chordwise loading of a wing
2. The nuanced shape of the leading-edge affects the shape of the pressure distribution, interaction between the pressure profile and the geometry, in turn define the magnitude of leading-edge-suction
3. Accurate computation of leading-edge-suction effects rely upon a very fine grid density computational model
4. Stronger leading edge suction leads to larger magnitude axial force coefficients, and
5. Negative axial force, reduces drag

Hence, sharp-leading edge airfoil wings – even with identical transverse span loads – will have higher drag-due-to-lift than blunt-leading-edge airfoil wings.

IV. Why Trefftz Plane Integrals Don't Work as Advertised

If the coarse grid of the Vortex-Lattice-Method solution precludes a direct pressure integration approach to induced drag, perhaps a wake-integral method would prove superior.

Earlier in this paper, we showed the flaw in Maskell's Method [11] – wings with equal shed bound vorticity will produce identical values of drag even though we just showed how sensitive axial force (and hence drag) is to the nuance of leading edge geometry irrespective of the span load.

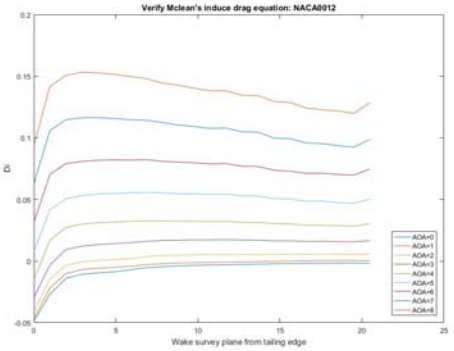

a

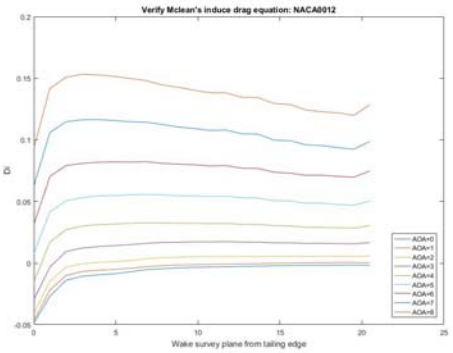

b

Figure 25: Influence of Sampling Plane Location for the Mclean Wake Integral

Here we ask if Mclean's approach would prove more sucessful. Recall, he suggested that induced drag is purely a measure of the extra kinetic energy found in the wake.

To investigate this using our CFD results, we used *TECPLOT* to interrogate the wake and integrate up the u, v, w perturbation velocities across a variety of cutting planes. We coded up his integral explored how Mclean's Di predictions varied as a function of trailing-edge to sampling plane distance. In Figure 25, we present our results: we found a strong distance-related effect present for both geometries and at all angles-of-attack. This is at odds with Brune [22] (using Maskell's Method [11]) who claimed that the lift and induced drag were independent from the downstream location of the wake survey.

We could also apply McLean's equations to a flow field survey developed using VORLAX. This has the advantage of producing a velocity field that could not possibly be contaminated with numerical dissipation effects (VORLAX is inviscid, and is a surface-panel representation). Here we examined the choice of the cutting plane orientation. We wondered how the integral would vary as we changed the alignment of cutting plane from: 1) the incoming wind frame, 2) to in a mean downwash

aligned frame or 3) the body reference frame. Turning to Figure 26, we see that there is little quantative difference.

Turning to Figure 27, we explored the values of the Mclean wake integral applied to both CFD and VORLAX wake fields.

Let us begin with Figure 27a; the NACA 0012 wing. Here, we found that the CFD flow-field derived wake integral substantially underpredicted the drag-due-to-lift; whereas the VORLAX flow-field derived wake integral and the VORLAX flat-plate with analytical leading-edge-suction correction only slightly underpredicted the drag-due-to-lift. From this, we could argue that the VORLAX's wake-integral closely matches the analytical correction. The CFD drag-due-to-lift is higher - around 10%-20% more - which we can treat as the influence of separation. However, the large discrepancy between the surface pressure and traction integrated drag and the wake-integral drag indicates that something is fundamentally unhappy with Mclean's integral.

Turning to Figure 27b reveals more trouble; this is the Biconvex wing. As expected the sharp-leading-edge wing has much higher drag-due-to-lift than $CL^2/\pi AR$. However, none of this is found in the Mclean integral of the CFD wake. In fact the Mclean integral from the Biconvex data closely matches the Mclean wake-integral from the 0012 solution.

Taking Figures 26 and 27 together, we an alarming trend – according the the Mclean wake integrals there was little substantive difference between the sharp and blunt-leading-edge wings.

Thus, we sadly conclude that Mclean's method (like Maskell's method) only captures effects of transverse loading - it doesn't fundamentally capture the leading-edge suction effect.

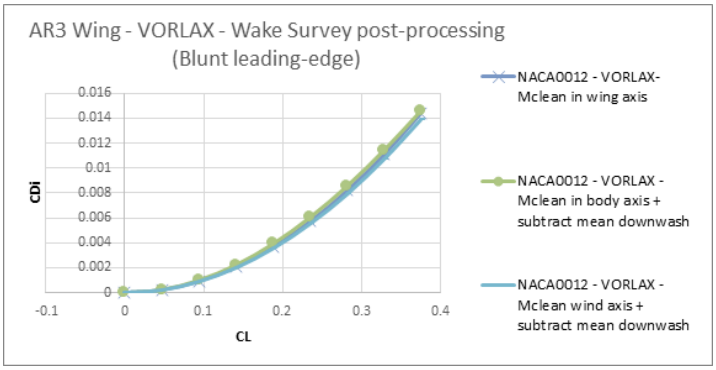

Figure 26: Influence of Cutting Plane Geometry on the Mclean Wake Integral

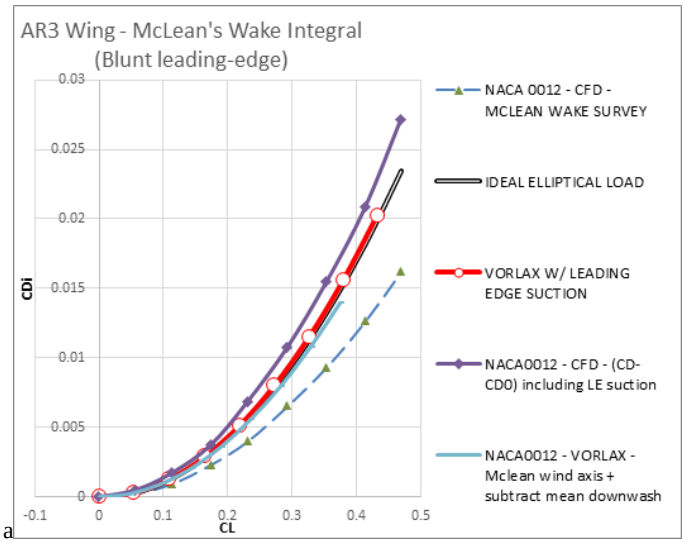

a

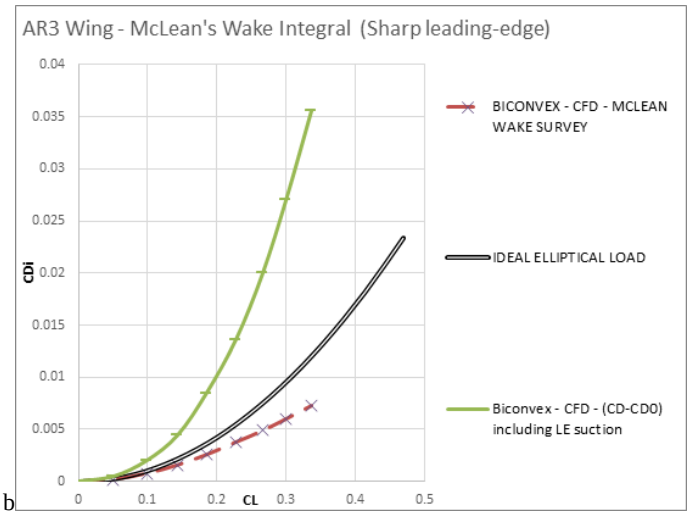

b

Figure 27 – Mclean wake integral for NACA 0012 and Biconvex sections

V. Discussion & Conclusions

We find the weakness of Mclean's wake-integral formula [11] especially troubling because, like Betz [25] it is so physical and so intuitive. If it is "wrong," it places into question the entire basis of control volume analysis.

What we came to understand was that control volume analysis can be (and is usually) evaded by a classic blunt-leading-edge wing. We came to this conclusion because Mclean defines the kinetic energy losses in the wake as a proxy for lift-induced-drag. Based on Kelvin's circulation theorem, the energy of the shed vortex is equal to the bound vortex and the bound vorticity is the one to generated lift to each panel. The key here is that while blunt and sharp leading-edge wings might have the same or similar bound vorticity, differences in leading-edge geometry mean that they apportion normal and axial forces with widely different ratios (see Figure 28).

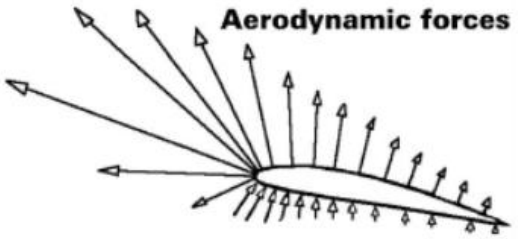

Figure 28 - Pressure Forces – How Geometry Apportions this between Normal and Axial Forces

In other words, we can see the wake survey as:

```
Wake Integration = the energy of shed vortex = the energy of bound vortex

= the sum of lift on each panel = normal vector of some panels is pointed to vertical direction, but some is points to horizontal direction.

= energy to generated lift (wing axis) + energy to generated leading-edge thrust.

= vortex-drag (+) + leading-edge suction (-).

Total drag = vortex-drag + leading-edge suction (-) + profile drag.
```

Mclean [11] emphasizes that induced drag is a measure of the shed vorticity in the wake. Based on the development of these theories, Mclean believes the energy loss in the wake goes back to the consequence of lift because of the energy conservation and Kelvin's theorem. His logic is correct, but we know the source of his theory is the Kutta-Joukowski theorem which assumes the airfoils have round leading-edge and sharp trailing-edge (with Kutta condition). In this perspective, Mclean's method also neglects the thickness effect and presumes all wings have a blunt leading and sharp trailing edges. Like the classical methods, it contrives an induced drag formula accurate only for ideal blunt leading-edge wings.

If the reader remains troubled with this heresy, we point him back to the classics and remind him that those derivations fundamentally neglect thickness. They rotate normal forces into the drag direction. They do not consider the curvature or thickness of the surface; they are based on an idea that pressure forces are always pointed orthogonal to the airfoil mean-line. They assume all airfoils derive from a geometric transformation of perfect, inviscid flow around a cylinder. Thus, in this idealized world, the sum of pressure forces on the surface of a circle in the drag direction is identically zero. This property of ideal inviscid flow means that all follow-up theories developed from the Kutta-Joukowski theorem make the same assumption: the airfoils don't have thickness effects and cannot develop axial forces due to inviscid flow mechanisms.

Our viscous and inviscid test data (computation and experiment) show that these wake surveys don't predict real-world drag.

Ultimately, we come to show that the Vortex-Lattice-Method is an effective computational code for aircraft design, but that such codes must be used carefully.

- Thin flat plate panel models with analytical leading-edge-suction corrections can be used to accurately infer the induced drag-due-to-lift of complex configurations (100% correction for blunt-leading edges, somewhat less ~30% for the biconvex section).

- Sandwich panel models cannot be used to induced-drag computations, but they can be used to generate detailed geometry (including thickness, camber and twist distributions) to match target streamwise pressure distributions and transverse span load distributions.

- CFD models, while tedious to generate, can be used to verify and validate panel method solutions. Lift and drag estimates made using direct surface pressure and traction integration are accurate.

and

- For any source (CFD, VLM or Wind Tunnel), the Trefftz plane wake-integral is much less useful than generally assumed – especially for aircraft with unusual leading edge geometry

ACKNOWLEDGEMENTS

This unsponsored work was performed by Mr. Ou in partial fulfillment of the degree requirements for obtaining a M.S. in Aerospace Engineering at Arizona State University. [32] We thank undergraduate student's Martin Morrow [29] and Galen Kingsley [30] for their respective experimental work in the Arizona State University undergraduate wind tunnel.

REFERENCES

[1] Lamar, J. and Margason, R., "Vortex Lattice FORTRAN program for estimating subsonic aerodynamic characteristics of complex planforms," NASA TN D-6142, p. 20, 1971.
[2] *See:* https://en.wikipedia.org/wiki/Vortex_lattice_method
[3] Ashley, H. and Landahl, M., *Aerodynamics of Wings & Bodies*, Addison Wesley, Reading, Mass. USA, 1965.
[4] Etkin, *B.* and Reid, L.D., *Dynamics of Flight*, 3rd edition, Wiley, 1995.
[5] Miranda, L. R., Elliot, R.D. and Baker, W.M., "A generalized Vortex-Lattice-Method for subsonic and supersonic flow applications," NASA CR-2865, 1977.
[6] *See:* http://web.mit.edu/drela/Public/web/avl/
[7] *See:* https://starkaerospace.com/products-services/ami/software/
[8] *See:* http://tornado.redhammer.se/
[9] El Haddad, N.R. & Gonzalez, L., "Aerodynamic Design of a Winglet for the Dassault Falcon 10," AIAA 2016-0776, 2016.
[10] Munk, M.M., *Fundamentals of Fluid Dynamics for Aircraft Designers*, self published, 1933.
[11] McLean, D., *Understanding aerodynamics : arguing from the real physics*. Wiley-Blackwell, 2013.
[12] Larrabee, E., "The aerodynamic design of sailplane tail assemblies," Tech. Soar., vol. 5, no. 1, pp. 21–28, 1976.
[13] Küchemann, D., "Investigation of the lift distribution over the separate wings of a biplane," NASA Tech. Rep., no. 889, 1939.
[14] Anderson, J.D. , *Fundamentals of Aerodynamics*, McGraw-Hill Education, 2010.
[15] Bertin, J. and Cummings, R., *Aerodynamics for Engineers*. Prentice Hall, NJ, 2002.
[16] Katz, J. and Plotkin, A., *Low-Speed Aerodynamics*. Cambridge University Press, 2001.
[17] Joukowsky, N., "Über die Konturen der Tragflächen der Drachenflieger," vol. 1, pp. 281–284, 1910.
[18] Kuethe, A.M. and Schetzer, J.D., *Foundations of Aerodynamics*. 1959.
[19] Drela, M., *Flight Vehicle Aerodynamics*. MIT Press, 2014.
[20] Multhopp, H., "Methods for calculating the lift distribution of wings (subsonic lifting-surface theory)," ARC R&M No. 2884, 1955.
[21] Maskell, E.C., "Progress Towards a Method for the Measurement of the Components of the Drag of a Wing of Finite Span," Royal Aircraft Establishment, TR 72232, UK, Dec. 1972.
[22] Brune, G.W. and Bogataj, P.W., "Induced drag of a simple wing from wake measurements," SAE Tech. Pap. 901934, pp. 1889–1901, 1990.
[23] Brune, G.W., "Quantiative Low Speed Wake Surveys," AIAA J. Aircraft, Vol 31, No. 2, 1994.

[24] Smith, S.C. “A computational and experimental study of nonlinear aspects of induced drag,” NASA Tech. Rep. 3598, pp. 89–92, 1996.
[25] Betz, A.“A method for the direct determination of wing-section drag,” NACA TM-337, 1925.
[26] Takahashi, T.T., “On the decomposition of drag components from wake flow measurements,” AIAA 97-0717, 1997.
[27] Bairstow, L. and Jones, B. Melvill, “Experiments on models of aeroplane wings,” ARC R&M, No. 60, 1912.
[28] “Turbulent model for Autodesk CFD,” 2016. [Online]. Available: http://www.autodesk.com/products/cfd/features/all/list-view.
[29] Kingsley, G.P., “Wind Tunnel Test Data of an Untapered Aspect Ratio 4 0015 Wing, Unpublished Raw Data,” 2018.
[30] Morrow, M.H., “Leading Edge Geometry Effects on Pressure Drag and Pressure Thrust for Various Wing Geometries,” 2017.
[31] Lan, C.E. “A Quasi-Vortex-Lattice Method in Thin Wing Theory” AIAA J of Aircraft, Vol 11, No. 9, p 518-529, 1974.
[32] Wei, C.-W. M.S. Thesis, Arizona State University, 2019.